Electrochemical Deposition and Reoxidation of Au at Highly Oriented Pyrolytic Graphite. Stabilization of Au Nanoparticles on the Upper Plane of Step Edges

Chett J. Boxley and Henry S. White*

Department of Chemistry, University of Utah, 315 S. 1400 E., Salt Lake City, Utah 84112

Tedd E. Lister and Patrick J. Pinhero

Idaho National Engineering and Environmental Laboratory, P.O. Box 1625, Idaho Falls, Idaho 83415

Received: July 10, 2002; In Final Form: October 9, 2002

The electrochemical deposition and reoxidation of Au on the basal plane of highly oriented pyrolytic graphite (HOPG) immersed in a 5 mM $AuCl_4^-$/6 M LiCl solution is reported. Scanning electron microscopy (SEM) and ex-situ atomic force microscopy (AFM) demonstrate that Au nanoparticles, ∼3.3 nm in height and ∼10 nm in diameter, are deposited at times less than ∼1 s. The density of nanoparticles, 6×10^9 cm^{-2}, is of the same order of magnitude as the surface point defect density, suggesting that point defects act as nucleation sites for Au electrodeposition. A small subset of the Au nanoparticles (∼7%) continues to grow between 1 and 50 s, reaching a height of ∼150 nm and a diameter of ∼300 nm. At times greater than 50 s, the larger particles coalesce to yield a surface comprised of a low density ($\sim 2 \times 10^6$ cm^{-2}) of micrometer-size Au crystallites surrounded by Au nanoparticles. Double potential step chronocoulometric experiments demonstrate that the electrodeposition of Au is chemically irreversible, a finding supported by SEM and AFM observations of Au nanoparticles and larger crystallites on the surface after long periods of reoxidation (>3600 s). Au nanoparticles are observed to be preferentially deposited on the upper plane of step edges, a consequence of the nonuniform surface electron density that results from relaxation of the graphite lattice near steps.

Introduction

A fundamental goal in the science of electrochemical deposition is to understand the structural relationship between a deposited material and the interface at which it is deposited. Much progress has been made in the past two decades in understanding how the periodic structure of single crystal electrode surfaces influences the orientation and energetics of metal, molecular, and anion overlayers, especially in the underpotential deposition (upd) of mono- and bi-layers of metal atoms on a foreign metal surface.[1] In contrast, the role that nonideal interfacial structures (e.g., steps, point vacancies, and adsorbates) play in the electrodeposition processes is significantly less well studied, in part, due to the fact that defect sites represent a minuscule fraction of the surface area and, thus, are difficult to identify and characterize.[2−4] While it is generally understood that imperfections in a crystallographic surface plane will influence electrochemical nucleation rates and the morphology of the deposited film, very few studies have attempted to characterize this relationship, even at the most qualitative level.

In the present report, we describe an investigation of the deposition of Au nanoparticles on the basal surface of highly ordered pyrolytic graphite (HOPG). We have attempted to identify, using ex-situ atomic force microscopy (AFM), the specific surface defect structures that act as sites for particle nucleation. The atomically smooth exposed surface of HOPG electrodes contains a relatively high density of defect structures that dominate the behavior of this electrode material. For instance, larger defects, e.g., steps and monolayer deep pits in the graphite surface, are known to serve as nucleation sites for the electrochemical deposition of polymers,[5] metals,[6] and metal oxides.[7] Especially relevant to our investigations are recent seminal reports by Penner and co-workers in which the intrinsic defect structure of HOPG is exploited to synthesize metal oxide nanowires and metal nanoparticles.[6−9] Similar to previous studies of metal deposition on HOPG, our studies demonstrate that Au nanoparticles are preferentially deposited along step edges and at intrinsic point defects. However, AFM images presented here unequivocally demonstrate that deposition occurs exclusively on the upper plane of the step edge, a finding that runs counter to currently accepted models of electrodeposition. The origin of metal nucleation on the upper plane of step edges is discussed in terms of the influence of nonuniform surface electron density near surface defects.

A second aspect of this work concerns the stability of Au nanoparticles, following their deposition onto the HOPG basal plane. While a number of fundamental studies concerning the mechanism of Au electrodeposition at different substrates, e.g., Pt,[10] n-Si,[11] and Au[12,13] and HOPG,[14−16] have been reported, very little attention has been given to the reoxidation of electrodeposited Au.[12] We observe that the Au nanoparticles deposited on HOPG exhibit an unusually high stability toward reoxidation, persisting for indefinite periods at electrode potentials where larger Au particles (as well as bulk Au) are readily oxidized. Ng and Penner have reported a similar behavior of Ag nanoparticles on HOPG.[6] Although the origin of this behavior is not understood, our present results, and those of Ng and Penner, demonstrate that new patterns of electrochemical behavior emerge when the metal particle dimensions are reduced to the nanometer scale.

* Author to whom correspondence should be addressed.

10.1021/jp026496j CCC: $25.00
Published on Web 12/18/2002

Experimental Section

Cyclic voltammetry and double potential step chronocoulometry were performed employing a Princeton Applied Research (PAR) model 175 universal programmer, a model 173 potentiostat/galvanostat, and a model 179 digital coulometer/current follower. Data were recorded using virtual instrumentation written in National Instruments LabVIEW.

Electrochemical experiments were performed using a 3-electrode cell. The HOPG working electrode was mounted onto a stainless steel base using Ag paint; a Teflon cell with an opening in the bottom was pressure fitted against the HOPG surface using an O-ring (Hydra Pak Seals, i.d. 0.602 cm) to expose an active electrode surface of 0.28 cm^2. A Ag/AgCl (3 M NaCl) reference electrode and a Pt wire auxiliary electrode were employed throughout; all electrode potentials are reported using the Ag/AgCl scale.

$HAuCl_4$ (Alfa Aesar, 99.99%) and LiCl (Mallinckrodt, 99.7%) were used as received. Water was purified by use of a Barnstead E-pure 4-module ORGANICfree system. HOPG (Advanced Ceramics, ZYB and ZYC grade) was freshly cleaved with sticky tape to expose a fresh surface prior to each experiment. Thermally etched HOPG samples were prepared by heating a freshly cleaved sample in air at 650 °C for 10 min. using a Thermolyne type 21100 tube furnace.[17−19]

AFM images were recorded with a Molecular Imaging PicoScan system (MI Inc., Tempe, AZ), operated in magnetic AC (MAC) noncontact mode, and using AFM tips coated with a magnetically conductive material (MI Inc., type II MAC tips). The cantilevers were 3 μm-thick monolithic doped Si with a force constant of 1.2−5.5 N/m and a resonance frequency of 60−90 kHz. Tip radii are reported by the manufacturer to be less than 10 nm. Images were recorded using either the AFM "M" piezo scanner with a maximum scan range of 30 μm × 30 μm, or the AFM "S" piezo scanner with a scan range of 6 μm × 6 μm. All experiments were performed within an acoustically isolated cabinet, with the scanner positioned on a surface suspended with elastic cords. Images were recorded using both height and deflection mode. In height mode, the movement of the *z*-piezo necessary to maintain a constant cantilever oscillation is recorded. In deflection mode, the derivative of the height mode signal is acquired simultaneously. The deflection mode signal is a measure of the amplitude change in the oscillation of the cantilever caused by variations in the surface topography. Most of the AFM images reported in this article are deflection mode images.

SEM images were obtained using a Philips type 30 Environmental SEM operating at vacuum pressures between 10^{-6} − 10^{-7} Torr. Typical conditions included a 20 kV accelerating voltage and a 16-mm working distance. This instrument is able to resolve Au particles having dimensions greater than ∼30 nm.

Results and Discussion

Electrochemical Behavior of HOPG in 5 mM $AuCl_4^-$/6 M LiCl Solutions. A brief overview of the electrochemical behavior of HOPG electrodes in the 5 mM $AuCl_4^-$/6 M LiCl solution is presented here prior to discussing the structural analysis of the electrodeposited Au particles. The predominant valence state of Au in this solution is Au(III);[10,15,20] however, a small amount of Au(I) may be present in solution due to the disproportionation between electrodeposited Au(0) and Au(III) (i.e., $AuCl_4^- + 2Au + 2Cl^- \rightleftharpoons 3AuCl_2^-$).[15]

Figure 1A shows the cyclic voltammetric response (first scan at 20 mV/s) of an HOPG electrode in an unstirred 5 mM $AuCl_4^-$/6 M LiCl solution. The reduction of the Au(III) species

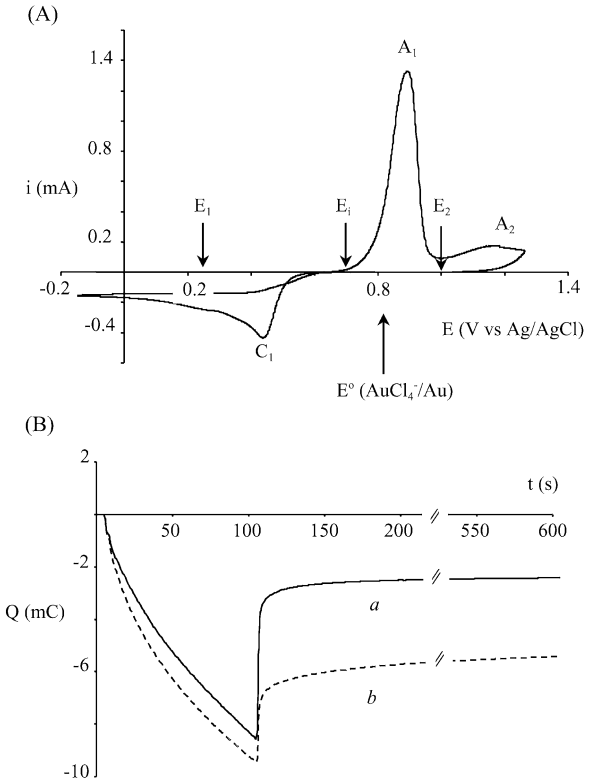

Figure 1. (A) Cyclic voltammetric response of an HOPG electrode in an unstirred 5 mM $AuCl_4^-$/6 M LiCl solution. The electrode potential was scanned, beginning at 0.80 V vs Ag/AgCl, in the negative direction at 20 mV/s. (B) Background subtracted double-potential step coulometry plots of charge (Q) versus time (t) for (a) freshly cleaved, and (b) thermally etched HOPG electrodes during electrodeposition and reoxidation of Au. The initial potential step at $t = 0$ s was from $E_i = 0.72$ V to $E_1 = 0.25$ V, resulting in the electrodeposition of Au. The reverse potential step at $t = 100$ s was from $E_1 = 0.25$ V to $E_2 = 1.0$ V, resulting in the partial reoxidation of electrodeposited Au.

is characterized by a single cathodic peak at 0.44 V (labeled C_1) that corresponds to the overall 3-e^- transfer, eq 1. The microscopic mechanism of Au

$$\mathrm{Au(III)} + 3e^- \rightleftharpoons \mathrm{Au(0)} \qquad (1)$$

deposition is clearly more complex than the overall reaction in eq 1, involving adsorbed Au complexes of intermediate valencies. However, the focus and conclusions of this report do not require assumption of a specific mechanism.

The standard reduction potential for the Au(III)/Au(0) couple, $E°$, is 0.804 V vs Ag/AgCl.[15] Figure 1A shows that the onset of Au reduction on HOPG begins at 0.57 V, approximately 0.23 V *negative* of $E°$. The 0.23 V difference represents the overpotential for Au nucleation on HOPG, and is in good agreement with values reported previously for Au electrodeposition onto HOPG.[10,14,15] The hysteresis observed during the reverse potential scan is characteristic of slow nucleation followed by diffusion controlled growth of the Au deposits.[10,14,15]

Reoxidation of the electrodeposited Au on the reverse positive going scan is associated with anodic peaks at 0.89 and 1.16 V (labeled A_1 and A_2, respectively, in Figure 1A). Similar multiple anodic peaks have been previously reported by Osteryoung and co-workers for the voltammetric reoxidation of electrodeposited Au at HOPG electrodes.[15] These researchers assigned the first anodic peak (A_1) to a 3-e^- oxidation, but did not discuss the smaller second anodic peak (A_2). However, Welham and co-

TABLE 1: Percentage of Au Re-oxidized at Freshly Cleaved and Thermally Etched HOPG

	@ 0.90 V[b]	@1.00 V	@1.20 V
freshly cleaved HOPG	51 ± 8%[a,c]	73 ± 4%	83 ± 5%
thermally etched HOPG	26 ± 12	42 ± 14	50 ± 10

[a] Percentages determined from double potential step chronocoulometric measurements. Au was initially deposited for 100 s at $E = 0.25$ V vs Ag/AgCl, and then reoxidized for 100 s at the indicated potential. The percentage of reoxidized Au is defined as the ratio of the anodic charge, Q_a measured during reoxidation relative to the cathodic charge, Q_c, measured during electrodeposition (× 100). [b] vs Ag/AgCl. [c] All values are based on 10 to 13 independent measurements using different electrodes. Uncertainties represent one standard deviation from the mean.

workers observed multiple anodic peaks for the reoxidation of Au at polycrystalline Pt, assigning peak A_1 to a multistep $3e^-$ transfer and peak A_2 to a direct 3-e^- transfer.[10]

Voltammetric measurements of Au deposition were also performed using thermally etched HOPG surfaces in order to explore the dependence of nucleation overpotential on surface defect structure. Thermal etching of the HOPG surface results in an increased density of exposed step edges and pits.[17] Electron-transfer reactions between soluble redox species and the HOPG surface are ~2 orders of magnitude more facile at these surface imperfections relative to the basal plane,[21] a difference attributed to a higher conductivity along the in-plane axis.[22] Edge sites have also been previously shown to act as nucleation sites for the electrochemical deposition of polymers[5] and metals.[6,7] Our results indicate that there is no reproducible difference in the cyclic voltammetric responses of freshly cleaved and thermally etched HOPG surfaces. However, as shown below, step edges exert a significant influence on the stability of the Au nanoparticles.

Double potential step chronocoulometry was used to determine the chemical reversibility of Au electrodeposition on HOPG, eq 1. Figure 1B shows double-step chronocoulometric responses (charge (Q) vs time (t)) recorded using freshly cleaved (curve a) and thermally etched (curve b) HOPG electrodes in the 5 mM $AuCl_4^-$/6 M LiCl solution. In these experiments, the electrode potential is stepped from an initial potential where no reaction occurs ($E_i = 0.72$ V, marked on the voltammetric curve in Figure 1A) to a potential where $AuCl_4^-$ is reduced at a diffusion controlled rate ($E_1 = 0.25$ V). The electrode potential is held at E_1 for a deposition time of 100 s while the Q vs t response is recorded. In the second part of the experiment, the electrode potential is stepped from E_1 to a potential where the electrodeposited Au is reoxidized ($E_2 = 1.00$ V). Background Q vs t responses obtained in a 6 M LiCl solution for each electrode were subtracted from the responses in the presence of $AuCl_4^-$.

Inspection of the chronocoulometric responses in Figure 1B demonstrates that electrodeposition is chemically irreversible on the time scale of the reoxidation step (600 s for the data reported in Figure 1B); i.e., a significantly smaller charge is recorded during the reoxidation step than is recorded during electrodeposition. Based on measurements using 10 different electrodes, only 73 ± 4% of electrodeposited Au is reoxidized at the freshly cleaved HOPG, Table 1. A significantly smaller fraction (42 ± 14% based on 13 different electrodes) of Au is reoxidized at thermally etched HOPG electrodes, suggesting that step edges on the HOPG surface promote the stabilization of Au particles against oxidation. Table 1 summarizes the percentage of Au that is reoxidized at oxidation potentials between 0.9 and 1.20 V. As expected, the amount of Au that is reoxidized

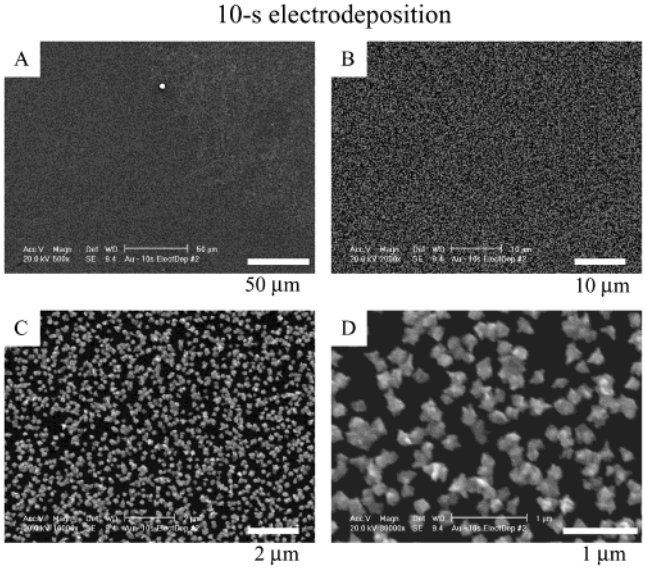

Figure 2. SEM images of Au following electrodepostion for 10 s at $E_1 = 0.25$ V vs Ag/AgCl. Images (A) through (D) correspond to progressively higher magnifications of the same surface region. The deposition conditions are the same as in Figure 1.

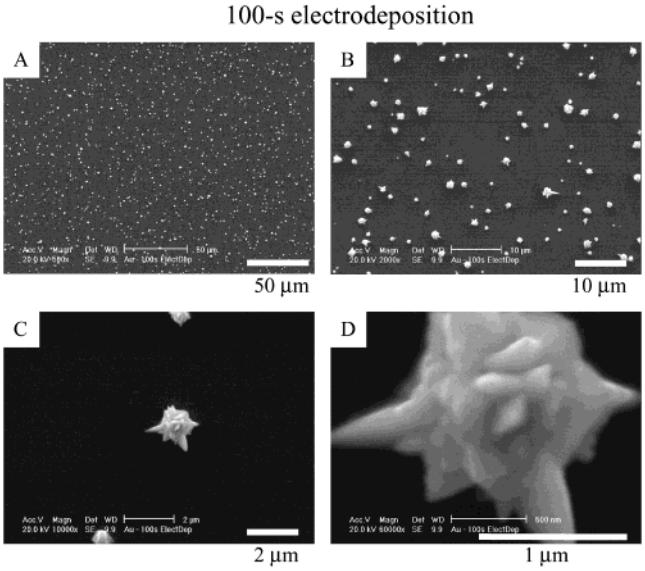

Figure 3. SEM images of Au following electrodepostion for 100 s at $E_1 = 0.25$ V vs Ag/AgCl. Images (A) through (D) correspond to progressively higher magnifications of the same surface region. The deposition conditions are the same as in Figure 1.

increases with increasing driving force; however, complete reoxidation of the electrodeposited Au is not observed.

The observed dependence of the chemical reversibility on the surface pretreatment of HOPG is somewhat surprising, our expectation being that the larger number of defect sites on a thermally etched surface would promote the reversibility of Au electrodeposition. The data in Table 1 demonstrate that electrodeposition is less reversible at the thermally etched surface, regardless of the driving force for oxidation. As shown in the following sections, Au nanoparticles in the close vicinity of step edges are indefinitely stable at electrode potentials where bulk Au is rapidly oxidized.

Electrodeposited Au Structures. SEM images of HOPG electrodes after electrodeposition of Au for 10 and 100 s, respectively, are shown in Figures 2 and 3. Energy dispersive spectroscopy (EDS) was used to confirm in all cases that the particles observed in the images are Au(0). Trace amounts of

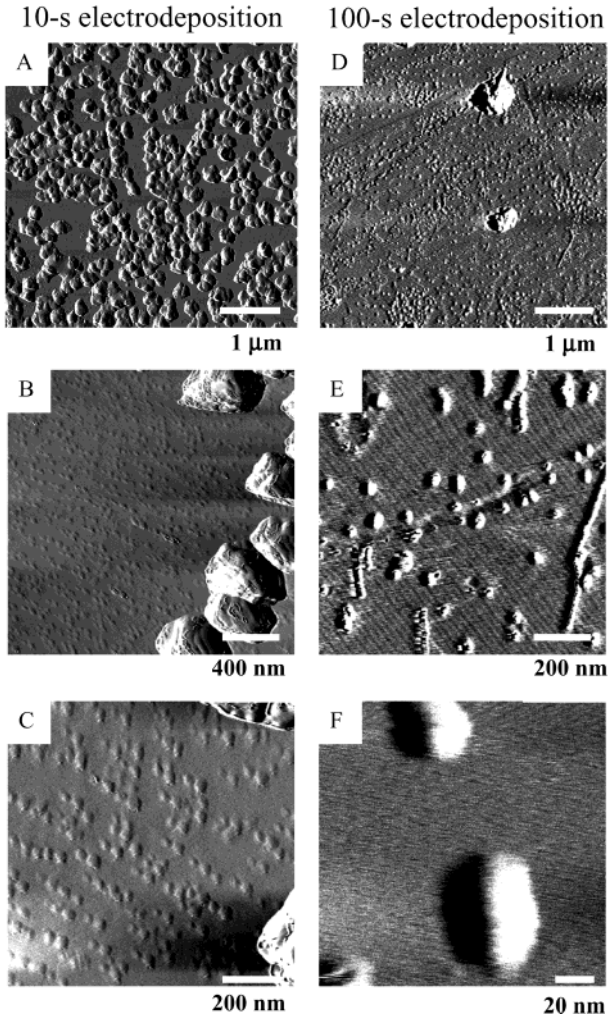

Figure 4. Ex situ AFM images of electrodeposited Au on freshly cleaved HOPG at $E_1 = 0.25$ V vsAg/AgCl. Images (A)−(C) correspond to a 10-s deposition and are progressively higher magnifications of the same surface region. Images (D)−(F) correspond to a 100 s deposition. Images (A)−(C) and (D)−(F) were obtained using different electrodes. The solution conditions are the same as in Figure 1.

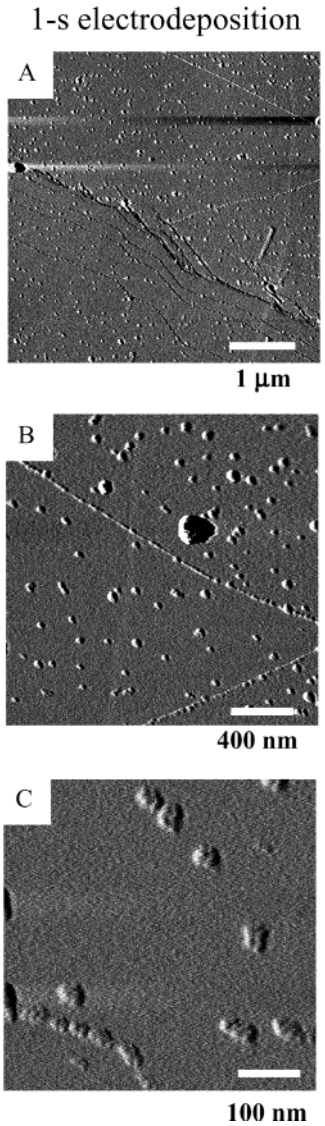

Figure 5. Ex situ AFM images of electrodeposited Au on freshly cleaved HOPG at $E_1 = 0.25$ V vsAg/AgCl. Images (A)−(C) correspond to a 1-s deposition and are progressively higher magnifications of the same surface region.

chloride on the Au particles could occasionally be detected by EDS. X-ray photoelectron spectroscopy also confirmed the presence of Au(0) on the surface, as well as trace amounts of chloride.

The SEM images presented in Figure 2 indicate that the electrodeposition of Au for 10 s results in a uniform coverage ($4 \pm 3 \times 10^8$ cm^{-2}) of faceted Au particles having relatively uniform size (~300 nm diameter). Surprisingly, the electrodeposition of Au for longer periods of time under identical conditions results in the *disappearance* of the majority of these submicrometer size particles and the generation of a low coverage ($2 \pm 2 \times 10^6$ cm^{-2}) of larger Au particles. For example, Figure 3 shows SEM images of a HOPG surface after a 100-s deposition. Comparison of the SEM images in Figures 2 and 3 demonstrates a nearly 2 orders of magnitude decrease in particle density at the longer deposition time, a finding reproduced in independent measurements using different electrodes and solutions.

Ex-situ AFM examination of the HOPG electrodes confirms the above-described differences in the surface density and size of the Au particles following 10-s and 100-s deposition periods. The AFM image presented in Figure 4A after a 10-s deposition shows Au particles ($4 \pm 3 \times 10^8$ cm^{-2}) that have uniform dimensions (150 ± 20 nm height and 300 ± 50 nm width), in good agreement with the size and distribution of the particles observed by SEM (Figure 2). Higher-resolution AFM images (Figure 4B and 4C) of the same surface region show that the surface is also decorated by a very high density of Au nanoparticles (3.3 ± 0.7 nm height; 32 ± 10 nm width) that are not resolved by SEM. Counting analysis of 3 HOPG surfaces following a 10-s deposition yields an average nanoparticle density of $6 \pm 3 \times 10^9$ cm$^{-2.}$ The AFM measured width probably represents the geometric convolution of the tip and particle (due to the sharp vertical relief), making these particles appear larger than their actual size. Although it is difficult to accurately de-convolute the influence of the tip, the particle diameter was estimated to be ~12 nm by subtracting the tip diameter (~20 nm) from the measured value.[23]

Figure 4D presents an AFM image of a HOPG surface after a 100-s deposition. Consistent with the SEM images in Figure 3, a low density of micrometer-size Au crytallites is observed at 100 s (only two of these larger particles are observed in Figure 4D). In addition, the surface is covered by Au nanoparticles similar to those observed after a 10-s deposition. AFM images recorded after a 1-s deposition, Figure 5, also reveal nanometer size particles at a surface density of $\sim 3 \times 10^9$ cm^{-2}.

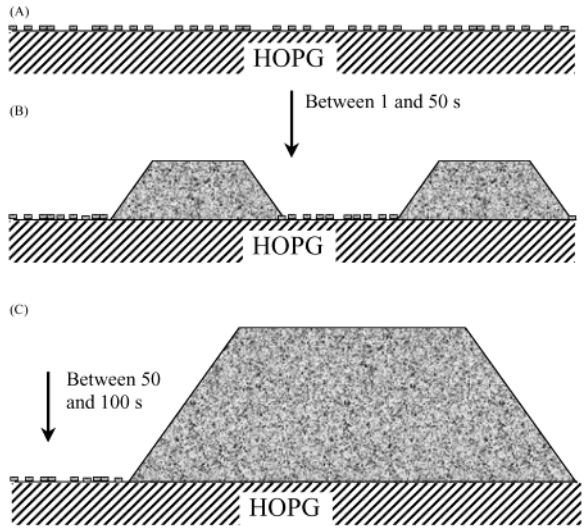

Figure 6. Qualitative representation of Au structures on HOPG for deposition times of (A) 1 s, (B) 10 s, and (C) 100 s. The structures are deduced from SEM and AFM images.

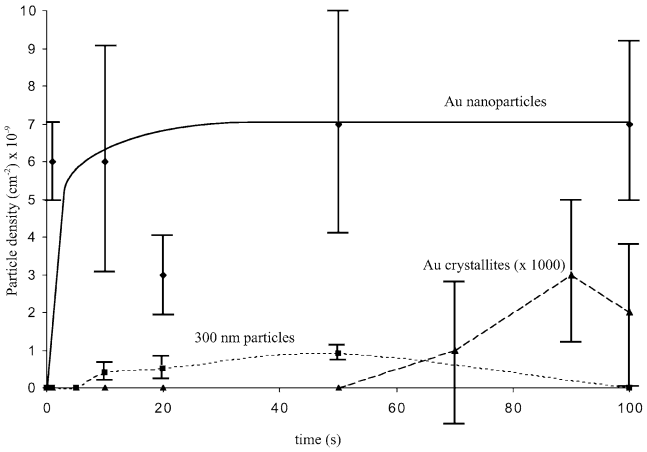

Figure 7. Plot of the surface particle density as a function of deposition time. Average values are based on number counts for different electrodes (typically 2) and for different regions (typically 3) of the same electrode.

Figure 6 shows a qualitative depiction summarizing the distributions and sizes of the Au particles based on SEM and AFM images at short (1 s), intermediate (50 s), and long (100 s) deposition times. The AFM images suggest that nucleation of a high density of Au nanoparticles (~3 nm height, ~10 nm width) on the basal plane occurs within ~1 s after initiation of electrodeposition. Interestingly, the number density of Au nanoparticles is slightly larger than the reported intrinsic point defect density on the basal plane of HOPG, $0.3-1.3 \times 10^9$ cm^{-2}, as previously estimated by counting the number of monolayer deep pits formed after thermal oxidation.[17−19,24] While this result suggests that nucleation of the Au nanoparticles may occur at preexisting point defects, a more systematic study employing surfaces with known defect densities is required to establish a definite relationship.

As depicted in Figure 6, a small fraction of the Au nanoparticles grow to intermediate size (300 nm width) between 1 and 50 s; the remaining nanoparticles (i.e., those not engulfed by the larger growing particles) do not undergo any significant growth during this time period. Figure 7 shows a plot of the time evolution of the number densities of different size Au particles (nanoparticles, intermediate size particles, and larger Au crystallites) over a 100-s deposition. The relatively large error bars (1 std. deviation) are due to the variation in the sample-to-sample particle densities. We believe that the large spread of particle densities reflects differences in the point defect density of individual samples of HOPG.

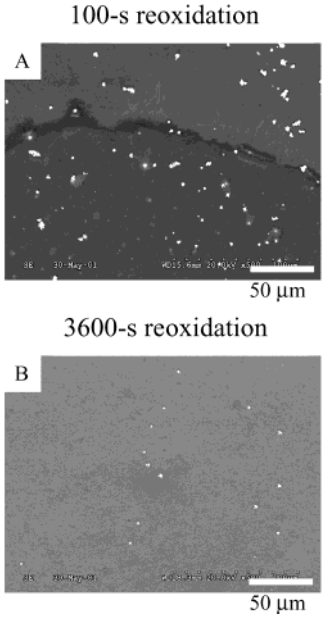

Figure 8. SEM images of Au remaining on the HOPG surface following reoxidation at $E_2 = 0.90$ V at (A) 100 s and (B) 3600 s. Au was initially deposited on each surface for a period of 100 s at $E_1 = 0.25$ V vs Ag/AgCl.

Particle density data collected from AFM images at electrodeposition times of 1, 5, 10, 20, and 50 s clearly show a bimodal distribution of particle sizes where a small subset (~7%) of the initially deposited nanoparticles grow with time while the remainder remain a constant size. A similar bimodal distribution of metal particles has been observed by Penner and co-workers during the electrodeposition of Ag at HOPG.[6] These researchers used Brownian dynamics simulations to demonstrate that the origin of the size bidispersity results from unequal fluxes of the metal ion to neighboring particles. Preferential growth occurs due to the larger particles receiving a greater portion of the total flux of $AuCl_4^-$ ions from the solution.[25]

SEM and AFM (Figures 2 and 3) indicate that a second structural transition occurs between ~50 and 100 s, resulting in the quantitative disappearance of the intermediate size particles and the formation of a small number of larger (>1 μm) Au crystallites. The density and size of the Au nanoparticles, however, are largely unaffected by this transition. The disappearance of the intermediate size Au particles, and appearance of larger crystallites, is most likely associated with the coalescence of the intermediate size particles, as the total mass of Au on the surface does not change significantly during this transition. The mechanism of this structural transition is not known.

Au Nanoparticles after Reoxidation. The chronocoulometeric response of the HOPG electrodes described earlier (Figure 1) suggests that Au electrodeposition in the 6 M LiCl solution is chemically irreversible, i.e., a significant fraction of the electrodeposited Au is not reoxidized at electrode potentials where oxidation of bulk Au is kinetically facile. SEM micrographs in Figure 8 show two HOPG electrodes after a 100-s deposition of Au, followed by reoxidation for 100 s (Figure 8A) and 3600 s (Figure 8B) at 0.90 V. Comparison of Figure 8A with images of HOPG electrodes prior to reoxidation of the Au (e.g., Figure 3) demonstrates that the majority of the

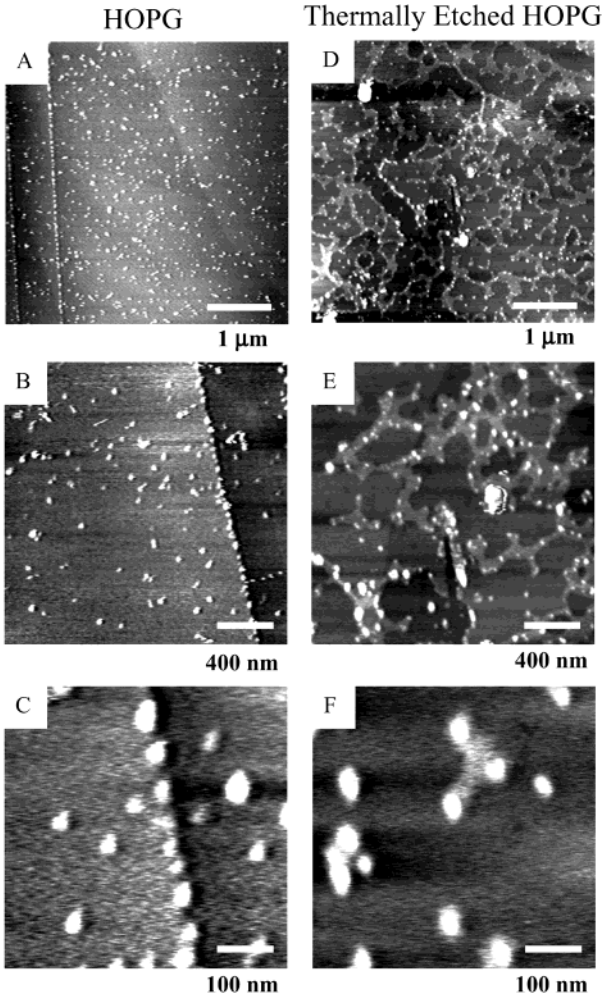

Figure 9. AFM images of Au nanoparticles on freshly cleaved (images (A)−(C)) and thermally etched (images (D)−(F)) following reoxidation at $E_2 = 0.90$ V for 100 s. Au was initially deposited on each surface for a period of 100 s at $E_1 = 0.25$ V vs Ag/AgCl.

larger Au crystallites (>75%) disappear within the first 100 s of reoxidation, suggesting that the electrooxidation of these structures is kinetically facile. However, small numbers of the large Au crystallites are occasionally observed in SEM images taken after a 3600-s reoxidation period, e.g., Figure 8B, clearly indicating the reoxidation and dissolution of these structures is not quantitative.

Higher-resolution AFM images of freshly cleaved and thermally etched HOPG electrodes following deposition and reoxidation are shown in Figure 9. For both samples, Au was electrodeposited for 100 s at 0.25 V, followed by reoxidization for 100 s at 0.90 V. The higher resolution AFM images show that Au nanoparticles are present on both surfaces. The density of the remaining nanometer size particles was found to be $3 \pm 1 \times 10^9$ cm^{-2}, about a factor of 2 lower than the observed density on most samples prior to reoxidation. The sizes of these particles (2.2 ± 0.8 nm, ~10 nm diameter) are equal, within experimental error, to the particle size prior to reoxidation. Similarly, the size of the nanoparticles on the thermally etched surface is essentially identical to the size of particles on the un-etched surface.

The coulometric charge measured during the deposition and reoxidation of Au, Figure 1B, is primarily associated with the larger, micrometer size crystallites, even though the density of these structures is 3 orders of magnitude lower than that of the Au nanoparticles. This conclusion is readily demonstrated by computing the amount of electrical charge associated with the nanometer size particles and the larger crystallites. On the basis of the initial nanoparticle density of $\sim 6 \times 10^9$ cm^{-2}, an average particle volume of 2.4×10^{-17} cm^3, and an electrode surface area of 0.28 cm^2, the total charge associated with the Au nanoparticles is ~6 μC. Thus, even 100% reoxidation of the nanoparticles can only account for ~0.1% of the anodic charge observed in the chronocoulometric experiments (for example, ~4 mC is passed during reoxidation using freshly cleaved HOPG, Figure 1B). On the other hand, the total charge associated with the larger crytallites is estimated to be ~8 mC (based on a density of $\sim 2 \times 10^6$ cm^{-2} and an estimated average particle volume of 1.0×10^{-12} cm^3). Thus, the charge passed during deposition and reoxidation oxidation is associated primarily with the larger crytallites.

The location of the electrodeposited Au nanoparticles is also very interesting. Au nanoparticles are observed along the top plane of the step edges and kink sites in every AFM image recorded of HOPG electrodes. Figure 9A−C shows an example of Au nanoparticles along the upper plane of a step edge on a freshly cleaved HOPG electrode. Although Au nanoparticles also randomly decorate the basal plane, it is clear that the nucleation of the particles is enhanced along the step edge. A similar phenomenon is observed in images of thermally etched HOPG, Figure 9D−F, where Au nanoparticles are located nearly exclusively on the upper plane adjacent to step edges. Close inspection of Figure 9D−F reveals that the location of Au nanoparticles is highly favored at the vertexes of graphite islands created by the thermal etching.

The tendency of the Au nanoparticles to deposit along the upper plane is in contrast to the "terrace-ledge-kink" (TLK) model[26] that suggests that metal particles should preferentially nucleate on the lower plane adjacent to a step edge.[7,27] A recent review by Nichols indicates that electrodeposition of a metal onto foreign and native metal substrates (e.g., Pb deposition on Ag, Au on Au, etc.) frequently follows predictions of the TLK model.[28]

The TLK model, however, does not correctly predict behavior of electrodeposited metals at HOPG. If a metal of interest is vacuum deposited and annealed on HOPG, then the resulting metal particles nucleate on the lower plane of an edge or kink site.[27,29−31] However, when metals are electrochemically deposited on the HOPG surface, particles frequently appear on the upper edge of an edge step or kink site.[6,9,14,23,32,33] A notable recent exception to this is the electrodeposition of the metal oxide, MoO_X, onto the lower plane of step edges.[7] To our knowledge, an explanation as to why electrodeposition at HOPG favors particle nucleation and growth on upper step planes has not been previously described.

The observed preferential deposition of Au nanoparticles on the upper plane of step edges is most likely associated with the influence of nonuniform surface electron density on the kinetics of particle nucleation. Both theoretical predictions and experimental observations of nonuniform surface electron density near point defects, step edges, and monolayer deep thermally etched pits on HOPG have been reported.[17,34−40] McDermott and McCreery reported atomic-resolution STM images that revealed the spacing between maxima in tunneling current increases from the normal 0.25 nm on the unperturbed basal plane of HOPG, to ~0.43 nm on the upper basal plane adjacent to a step edge,[34] extending as far as 85 nm away from a step edge.[34] These reseachers suggest that the observed disorder results from reaction of oxygen (or other molecular species) with dangling carbon sp^2 orbitals along the step edge, resulting in variation in

the electron density at the Fermi level.[37] While an adsorbate-induced perturbation of the electron density undoubtedly occurs, theoretical calculations suggest that the length scale of the perturbation is on the order of 3 nm.[37] Thus, it seems unlikely that the long-range structural disorder observed in STM images, as well as the preferential deposition of metal particles, is due purely to adsorbate chemistry at the step edge.

We speculate that a more likely source for a long-range electron density perturbation is the in-plane relaxation of the graphite layers away from the step edge. Because of the weak van der Waals interactions between graphite layers, when an atomic layer of graphite terminates at a step edge, slippage in the terminated plane in the direction away from the step edge is anticipated. While we are not aware of any calculations or measurement of how far such slips extend away from a one- or two-atom high step edge, slip transformations at larger steps over distances of 100 nm in length are readily observed in STM images.[41,42] We note that an in-plane slip of one cell unit results in a transformation of hexagonal graphite (ABABAB layered structure) to rhombohedral graphite (ABCABC layered structure). Although this structural transition does not involve any change in the in-plane arrangement of carbon atoms, the different layered structures (ABABA vs ABCABC) have sufficiently large differences in the Fermi level density of states that regions of rhombohedral and hexagonal graphite are easliy distinguished in STM images.[41,42]

The question then arises as to how a variation in the surface electron density might influence the electrochemical nucleation of metal particles. One simple explanation is that a localized higher electron density along the upper plane of the step increases the rate of electron transfer between the HOPG surface and $AuCl_4^-$ ions in solution, increasing the local rate of particle nucleation. Another scenario is that the surface electron density influences the adhesive energy between Au particles and HOPG, thereby directing nucleation where particles are most energetically favorable. Unraveling these mechanisms is complicated by the dependence of the surface electron density on applied electrode potential. Further studies are required in order to understand the factors that control nucleation of metal particles on HOPG.

Conclusions

The results of this study demonstrate that the electrodeposition of Au on HOPG from an unstirred $AuCl_4^-$/LiCl solution occurs by a mechanism involving the evolution of three distinct particle morphologies. A high density ($\sim 6 \times 10^9$ cm^{-2}) of Au nanoparticles, $\sim$3.3 nm in height and $\sim$10 nm in diameter, is deposited at times less than $\sim$1 s. The density of Au nanoparticles is comparable to the reported point-defect density on the basal plane of HOPG, suggesting that nucleation occurs at point defects. In the second phase of deposition, a small fraction ($\sim$7%) of the Au nanoparticles continue to grow for $\sim$50 s, reaching a maximum diameter of $\sim$300 nm, before coalescing, in the final stage, to form larger crytallites (>1 μm diameter). The final structure of the electrodeposited Au is a low density of large Au crytallites (with larger size dispersion) distributed throughout a high density of uniform-size Au nanoparticles.

A significant fraction of the Au nanoparticles appears to be stabilized against electrooxidation at potentials where bulk Au is thermodynamically unstable and readily oxidized. A similar phenomenon has been recently observed by Penner and co-workers, where Ag nanoparticles remained stabilized on the surface of HOPG for periods of hours under strongly oxidizing conditions.[6] The origin of this anomalous stability of Ag and Au nanoparticles remains unknown. Preferential deposition of the Au nanoparticles along the upper plane of step edges is also observed, suggesting that the nonuniform surface electron density created by termination of the graphite lattice tends to induce Au particle nucleation on the upper step edge plane.

We have not explored the reactivity of the Au nanoparticles in nonelectrochemical environments. However, a recent report by Zhu et al.,[43] demonstrated that the adsorption of molecular oxygen on Au nanoparticles in a vacuum is greatly enhanced relative to flat single crystal Au surfaces. We anticipate that the Au nanoparticles reported here may also exhibit other unusual reactivities and are currently exploring this possibility.

Acknowledgment. The authors thank Dr. Arthur Moore of the Advanced Ceramics Corporation for generously donating the HOPG used in this work and Prof. R. M. Penner (University of California−Irvine) for helpful discussions.. This work was supported by the Office of Naval Research (H.S.W.) and by the Department of Energy.

References and Notes

(1) Herrero, E.; Buller, L. J.; Abruna, H. D. *Chem. Rev.* **2001**, *101*, 1897.
(2) Staikov, G.; Lorenz, W. J. *Can. J. Chem.* **1997**, *75*, 1624.
(3) Holzle, M. H.; Zwing, V.; Kolb, D. M. *Electrochim. Acta* **1995**, *40*, 1237.
(4) Rooryck, V.; Reniers, F.; Buess-Herman, C.; Attard, G. A.; Yang, X. J. *Electroanal. Chem.* **2000**, *482*, 93.
(5) Snyder, S. R.; White, H. S.; Lopez, S.; Abruna, H. D. *J. Am. Chem. Soc.* **1990**, *112*, 1333.
(6) Ng, K. H.; Liu, H.; Penner, R. M. *Langmuir* **2000**, *16*, 4016.
(7) Zach, M. P.; Ng, K. H.; Penner, R. M. *Science* **2000**, *290*, 2120.
(8) Zoval, J. V.; Lee, J.; Gorer, S.; Penner, R. M. *J. Phys. Chem. B* **1998**, *102*, 1166.
(9) Zoval, J. V.; Biernacki, P. R.; Penner, R. M. *Anal. Chem.* **1996**, *68*, 1585.
(10) Diaz, M. A.; Kelsall, G. H.; Welham, N. J. *J. Electroanal. Chem.* **1993**, *361*, 25.
(11) Oskam, G.; Searson, P. C. *J. Electrochem. Soc.* **2000**, *147*, 2199.
(12) Gallego, J. H.; Castellano, C. E.; Calandra, A. J.; Arvia, A. J. *J. Electroanal. Chem.* **1975**, *66*, 207.
(13) Harrison, J. A.; Thompson, J. *J. Electroanal. Chem.* **1975**, *59*, 273.
(14) Martin, H.; Carro, P.; Hernandez Creus, A.; Gonzalez, S.; Salvarezza, R. C.; Arvia, A. J. *Langmuir* **1997**, *13*, 100.
(15) Schmidt, U.; Donten, M.; Osteryoung, J. G. *J. Electrochem. Soc.* **1997**, *144*, 2013.
(16) Liu, H.; Penner, R. M. *J. Phys. Chem. B* **2000**, *104*, 9131.
(17) Chang, H.; Bard, A. J. *J. Am. Chem. Soc.* **1991**, *113*, 5588.
(18) Chu, X.; Schmidt, L. D. *Surf. Sci.* **1992**, *268*, 325.
(19) Patrick, D. L.; Cee, V. J.; Beebe, T. P. J. *Science* **1994**, *265*, 231.
(20) Schmidt, U. C.; Osteryoung, J. G. *J. Electrochem. Soc.* **1997**, *144*, 3091.
(21) McCreery, R. L. *Carbon Electrodes: Structural Effects on Electron-Transfer Kinetics*; Bard, A. J., Rubenstein, I., Eds.; Marcel Dekker, Inc.: New York, 1995; Vol. 21.
(22) McDermott, M. T.; Kneten, K.; McCreery, R. L. *J. Phys. Chem.* **1992**, *96*, 3124.
(23) Zoval, J. V.; Stiger, R. M.; Biernacki, P. R.; Penner, R. M. *J. Phys. Chem.* **1996**, *100*, 837.
(24) Zhu, Y.; Hansen, T. A.; Ammermann, S.; McBride, J. D.; Beebe, T. P. J. *J. Phys. Chem. B* **2001**, *105*, 7632.
(25) Fransaer, J. L.; Penner, R. M. *J. Phys. Chem. B* **1999**, *103*, 7643.
(26) Stranski, I. N. *Z. Phys. Chem.* **1928**, *136*, 259.
(27) Yang, R. T.; Wong, C. *Rev. Sci. Instrum.* **1982**, *53*, 1488.
(28) Nichols, R. J. In *Frontiers of Electrochemistry*; Lipkowski, J., Ross, P. N., Eds.; Wiley-VCH: New York, 1999; pp 99−137.
(29) McBride, J. D.; van Tassell, B.; Jachmann, R. C.; Beebe, T. P. J. *J. Phys. Chem. B* **2001**, *105*, 3972.
(30) Wawro, A.; Kasuya, A.; Czajka, R.; Horiguchi, N.; Nishina, Y. *Surf. Coat. Technol.* **1994**, *67*, 173.
(31) Hovel, H.; Becker, T.; Bettac, A.; Reihl, B.; Tschudy, M.; Williams, E. J. *J. Appl. Phys.* **1997**, *81*, 154.
(32) Hendricks, S. A.; Kim, Y.; Bard, A. J. *J. Electrochem. Soc.* **1992**, *139*, 2818.
(33) Potzschke, R. T.; Gervasi, C. A.; Vinzelberg, S.; Staikov, G.; Lorenz, W. J. *Electrochim. Acta* **1995**, *40*, 1469.
(34) McDermott, M. T.; McCreery, R. L. *Langmuir* **1994**, *10*, 4307.

(35) Porte, L.; deVilleneuve, C. H.; Phanar, M. *J. Vac. Sci. Technol. B* **1991**, *9*, 1064.
(36) Albrecht, T. R.; Mizes, H. A.; Nogami, J.; Park, S. I. *Appl. Phys. Lett.* **1988**, *52*, 362.
(37) Mizes, H. A.; Foster, J. S. *Science* **1989**, *244*, 559.
(38) Sattler, K. *Int. J. Mod. Phys. B* **1992**, *6*, 3603.
(39) Soto, M. *Surf. Sci.* **1990**, *225*, 190.
(40) Kobayashi, K. *Phys. Rev. B* **1993**, *48*.
(41) Snyder, S. R.; Foecke, T.; White, H. S.; Gerberich, W. W. *J. Mater. Res.* **1992**, *7*, 341.
(42) Snyder, S. R.; Gerberich, W. W.; White, H. S. *Phys. Rev. B* **1993**, *47*, 10823.
(43) Zhu, Y.-J.; Schnieders, A.; Alexander, J. D.; Beebe, T. P. J. *Langmuir* **2002**, *18*, 5728.